HHS Public Access

Author manuscript

Oncogene. Author manuscript; available in PMC 2015 December 01.

Published in final edited form as:

Oncogene. 2015 June ; 34(25): 3273–3282. doi:10.1038/onc.2014.258.

TGF-β signaling alters the pattern of liver tumorigenesis induced by Pten inactivation

Shelli M. Morris[1], **Kelly T. Carter**[1], **Ji Yeon Baek**[2], **Amanda Koszarek**[1], **Matthew M. Yeh**[3], **Sue E. Knoblaugh**[4], and **William M. Grady**[1,5,*]

[1]Clinical Research Division, Fred Hutchinson Cancer Research Center, Seattle, WA 98109 USA

[2]Center for Colorectal Cancer, Research Institute and Hospital, National Cancer Center, Goyang, Republic of Korea

[3]Department of Pathology, University of Washington Medical School, Seattle, WA 98195 USA

[4]Comparative Medicine, Fred Hutchinson Cancer Research Center, Seattle, WA 98109 USA

[5]Department of Medicine, University of Washington Medical School, Seattle, WA 98195, USA

Abstract

Hepatocarcinogenesis results from the accumulation of genetic and epigenetic changes in liver cells. A common mechanism through which these alterations induce liver cancer is by deregulating signaling pathways. A number of signaling pathways, including the PI3K/PTEN/AKT and transforming growth factor β (TGF-β) pathways have been implicated in normal liver development as well as in cancer formation. In this study, we assessed the effect of the TGF-β signaling pathway on liver tumors induced by Pten (phosphatase and tensin homologue) loss. Inactivation of only the TGF-β receptor type II, *Tgfbr2*, in the mouse liver ($Tgfbr2^{LKO}$) had no overt phenotype, while inactivation of *Pten* alone ($Pten^{LKO}$), resulted in the formation of both hepatocellular carcinomas (HCC) and cholangiocarcinomas (CC). Interestingly, deletion of both *Pten* and *Tgfbr2* ($Pten^{LKO};Tgfbr2^{LKO}$) in the mouse liver resulted in a dramatic shift in tumor type to predominantly CC. Assessment of the PI3K/PTEN/AKT pathway revealed increased phosphorylation of AKT and GSK-3β in both the $Pten^{LKO}$ and $Pten^{LKO};Tgfbr2^{LKO}$ mice, suggesting that this pathway is constitutively active regardless of the status of the TGF-β signaling pathway. However, phosphorylation of p70 S6 kinase was observed in the liver of all three phenotypes ($Tgfbr2^{LKO}$, $Pten^{LKO}$, $Pten^{LKO};Tgfbr2^{LKO}$) indicating that the loss of Tgfbr2 and/or Pten leads to an increase in this signaling pathway. Analysis of markers of liver progenitor/stem cells revealed that the loss of TGF-β signaling resulted in increased expression of *c-Kit* and *CD133*. Furthermore, in addition to increased *c-Kit* and *CD133*, *Scf* and *EpCam* expression were also increased in the double knock-out mice. These results suggest that the alteration in tumor

[*]**Corresponding Author:** William M. Grady, MD Fred Hutchinson Cancer Research Center Clinical Research Division 1100 Fairview Ave. N, Mailstop D4-100 Seattle, WA 98109-1024 Phone: 206-667-1107 Fax: 206-667-2917 wgrady@fhcrc.org.

Conflict of Interest The authors declare no conflict of interest.

Supplementary Information accompanies the paper on the *Oncogene* website (http://www.nature.com/onc).

types between the *Pten*^{LKO} mice and *Pten*^{LKO};*Tgfbr2*^{LKO} mice is secondary to the altered regulation of stem cell features induced by the loss of TGF-β signaling.

Keywords

Liver cancer; AKT; hepatocellular carcinoma; cholangiocarcinoma; progenitor cells; c-Kit

Introduction

Worldwide, liver cancer is the second leading cause of cancer related deaths in men and sixth in women[1]. The high death rate is partially due to the fact that liver cancer is usually diagnosed after the tumor has metastasized. Hepatocellular carcinoma (HCC) accounts for about 70–85% of liver cancers and usually develops in the setting of chronic inflammation, usually secondary to hepatitis B or C or chronic alcohol abuse. Cholangiocarcinomas (CC) account for the majority of nonHCC liver cancers (10%). Notably, the incidence of intra-hepatic CC has been increasing over the last 30 years[2]. Additionally, rare tumors of mixed hepatocellular-cholangiocarcinoma (HCC-CC), which share features of both HCC and CC, have been identified[3]. Advances in our understanding of the molecular mechanisms involved in the formation of both HCC and CC are needed to develop more effective therapies for these cancers.

The deregulation of a number of intracellular signaling pathways has been implicated in liver cancer formation[4–8]. In addition to having a role in tumor formation, many of these pathways have been shown to play a role in the control of normal liver development and in the differentiation of liver cells (i.e. hepatocytes, cholangiocytes, oval cells, etc.). The PI3K/PTEN/AKT pathway is one such pathway[9,10]. In response to extracellular signals, the catalytic subunit of PI3K phosphorylates PIP_2 to generate the lipid second messenger, PIP_3, which regulates the activation of the PI3K signaling pathway through AKT. PTEN (phosphatase and tensin homologue), a lipid and protein phosphatase, dephosphorylates PIP_3, and inhibits PI3K signaling. As a result, PTEN controls the activation of the phosphatidylinositol-dependent kinase AKT and is a key regulatory component of this pathway. *PTEN* is frequently mutated in human tumors, which results in the constitutive activation of AKT and a subsequent increase in cell proliferation and inhibition of apoptosis[11]. Specifically, in human liver cancer, *PTEN* expression is suppressed in almost half of liver cancers and a subset of these cancers have mutant *PTEN* (4–5%)[12–14]. Multiple mouse models have shown that tissue-specific targeted disruption of *Pten* results in tumor formation in a variety of organs through a variety of mechanisms[15]. In the liver, one of the central effects of loss of *Pten* is the expansion of CD133+ liver progenitor cells and induction of steatohepatitis by 6 months of age[16,17]. It appears that injury caused by the loss of *Pten* induces the proliferation of Pten null bipotent progenitor cells, and eventually results in liver tumor formation in the mice by 12 months of age[16,18]. Deletion of *Akt2*, in the setting of *Pten* loss in the liver, can reduce proliferation of the liver progenitor cells and delay tumor development implicating PI3K pathway activation as an important mediator of cancer secondary to *Pten* inactivation[19].

In addition to PTEN and the PI3K signaling pathway, TGF-β and its family members including BMPs, activins, growth and differentiation factors (GDFs), and Nodal are also important for normal liver development and appear to have a complex role in liver cancer formation[5,20,21]. TGF-β ligands (TGF-β1, 2, and 3) are secreted cytokines that signal through heteromeric cell-surface complexes that consist of two transmembrane serine-threonine kinase receptors, TGFBR1 and TGFBR2. Activation of this receptor complex results in the recruitment and phosphorylation of receptor-regulated SMADs (R-SMADs) - SMAD2 and SMAD3. The activated R-SMADs then form a trimeric complex with SMAD4, translocate to the nucleus and regulate transcription. During fetal liver development, BMPs play a prominent role in liver bud commitment from cells in the ventral endoderm[22]. In addition, a gradient of TGF-β and activin signaling is important for cell specification and biliary differentiation during liver development[23]. TGF-β1 has also been shown to be involved in inducing hepatic differentiation of stem-cell like cell lines derived from adult rat livers, and activin A, BMP2 and BMP4 have been shown to play a role in hepatocyte differentiation of ES cells[24–26]. Furthermore, mouse model studies have shown that heterozygous deletion of the TGF-β pathway adaptor protein embryonic liver fodrin, ELF, leads to the development of HCC[27].

Like the PI3K/PTEN/AKT signaling pathway, there is substantial evidence implicating deregulated TGF-β signaling in liver cancer formation. However, in some specific instances, TGF-β appears to have the ability to act as either a tumor suppressor or as a tumor promoter, depending on the concurrent gene mutations and tissue microenvironment present in the cancer[28,29]. Therefore, in light of this complicated role of TGF-β signaling in liver cancer formation, we carried out a series of studies in mice to assess how liver cancer formation that occurs in the setting of inactivated Pten is affected by TGF-β signaling.

Results

Pten deletion in the liver results in tumor formation

Inactivation of PTEN is common in liver cancer with many liver cancers lacking PTEN expression secondary to mutations or other mechanisms, such as deregulated microRNA expression[30,31]. In this current study we set out to further characterize liver tumors in *Pten* null mice with and without functional *Tgfbr2*. To generate mice with *Pten* liver-specific knock-out ($Pten^{LKO}$), we crossed *Albumin-Cre* (*Alb-Cre*) transgenic mice with mice conditionally null for *Pten*[32,33]. Mice lacking *Alb-Cre* were used as a control. PCR analysis was used to confirm the genotypes of the mice (Supplementary Figure S1). Despite being born with no obvious phenotype, by 12–14 months of age, 67% of the $Pten^{LKO}$ mice developed liver tumors (Table 1). The liver to body weight ratio in the $Pten^{LKO}$ mice was increased nearly 3x compared to the control mice lacking *Alb-Cre* ($P < 0.0001$, Figure 1). This increase in liver weight is consistent with previous reports and is a reflection of the increased triglyceride accumulation and tumor burden that occurs in the absence of Pten[18]. Histological analysis of the primary tumors from the $Pten^{LKO}$ livers revealed the presence of hepatic adenomas (HADs), HCCs and CCs. Further analysis of the distribution of tumor types in individual $Pten^{LKO}$ mice showed that 3 mice (15%) developed HAD/HCC exclusively, 2 mice (10%) had only CCs, while 15 mice (75%) had a mixture of

HAD/HCC/CC tumor types (Table 1). In addition, many of the livers exhibited severe steatosis and biliary hyperplasia, as well as fibrosis and cholangiohepatitis. This observed tumor spectrum in our mice is consistent with a previous report that described the development of both HCCs and CCs in *Pten*^{LKO} mice at approximately 1 year of age[34].

Deletion of *Tgfbr2* in *Pten* null livers induces a shift in the histologic profile of the liver tumors

Liver specific disruption of *Pten* and *Smad4* in mice results in the induction of intra-hepatic CC by 4–7 months of age[34]. Smad4 acts as a convergent node in Smad mediated signaling in the signaling cascade initiated by TGF-β family members, including TGF-β, BMPs, activins, GDFs and Nodal. Since many ligands/receptors utilize Smad4, it is unclear as to what specific extracellular signal is responsible for mediating the induction of CCs vs. HCCs seen in the *Pten/Smad4* double knock-out mice. In light of prior data implicating TGF-β specifically in liver tumor formation, we generated a mouse model that lacks *Tgfbr2* in the liver. TGFBR2 is a mandatory component of the TGF-β receptor complex. Loss of Tgfbr2 results in deficient signaling by TGF-β1, TGF-β2, TGF-β3 and GDF15, but does not affect BMP, activin, Nodal and most GDF signaling[35]. The *Tgfbr2*^{LKO} mice were born healthy and did not develop any liver tumors by 15 months of age (Table 1).

To assess the effect of *Tgfbr2* deletion on tumor formation induced by Pten inactivation, livers from mice with both inactive *Pten* and *Tgfbr2* (*Pten*^{LKO};*Tgfbr2*^{LKO}) were generated. Approximately 86% of *Pten*^{LKO};*Tgfbr2*^{LKO} mice developed liver tumors by 14 months of age (Table 1). Similar to the *Pten*^{LKO} mice, the double knock-out mice also displayed an increase in the liver to body weight ratio compared to the control mice ($P < 0.0001$, Figure 1). Like, the *Pten*^{LKO} mouse model, HADs, HCCs and CCs were seen in the *Pten*^{LKO};*Tgfbr2*^{LKO} mice, however, the tumor type distribution was significantly different between the two genotypes. The *Pten*^{LKO};*Tgfbr2*^{LKO} mice had a profound biliary phenotype (Figure 2a and b). The livers in this genotype exhibited focal to multifocal CCs with marked biliary hyperplasia within the adjacent hepatic parenchyma. The biliary hyperplasia varied from proliferative, ectatic ducts to cystic bile ducts that were associated with mild fibrosis and inflammation. In contrast to the *Pten*^{LKO} mice, 11 *Pten*^{LKO};*Tgfbr2*^{LKO} mice (44%) developed CCs exclusively in their livers ($P = 0.0197$, Table 1). These CCs were characterized histologically by a mass-forming proliferation of infiltrating tubules and irregular glands lined by atypical biliary epithelial cells, abundant schirrous stroma and positive staining for the biliary epithelial cell marker, cytokeratin-19 (CK19) (Figure 2c and d).

A significant fraction of the *Pten*^{LKO};*Tgfbr2*^{LKO} mice (56%) had concurrent HAD/HCC and CC. Within both genotypes, most hepatocellular adenomas displayed loss of the normal hepatic lobular architecture and exhibited an irregular growth pattern and compression of the adjacent normal liver tissue. Some adenomas contained atypical large cells with abundant eosinophilic cytoplasm, large nuclei, and areas with numerous mitotic figures. HCCs in both models were poorly demarcated with irregular borders and focal invasion into the surrounding parenchyma (Figure 2e and f). The HCCs tended to be larger than the adenomas and often replaced nearly the entire hepatic lobe in which they were located. Cellular atypia

and mitotic figures were common. A subset of the HCCs were assessed for hepatocyte paraffin antigen-1 (HepPar-1) expression, and many expressed this protein, which labels hepatocytes and is generally used to distinguish HCCs from other tumor types[36] (Figure 2g and h). Interestingly, one *Pten*^{LKO};*Tgfbr2*^{LKO} mouse had a HCC metastasis to the lung (Figure 2i). The origin of the metastasis was confirmed with positive HepPar-1 staining (Figure 2j). No metastases were noted in the *Pten*^{LKO} mice.

In light of the early development of biliary hyperplasia and CCs in the *Pten/Smad4* double knock-out mice, we analyzed the livers from our mice at approximately 4–5 months of age. The youngest mice we assessed were 18 weeks old, and by this age, there were multiple regions of biliary hyperplasia in the *Pten*^{LKO};*Tgfbr2*^{LKO} mice (Figure 2k). Biliary hyperplasia was also seen in the *Pten* null mice, but to a slightly lesser extent (Figure 2l).

We also determined the distribution of the different tumor types in the *Pten*^{LKO} and *Pten*^{LKO};*Tgfbr2*^{LKO} mice. A total number of 157 tumor sections from the *Pten*^{LKO} mice were reviewed. We found that 34% of the tumors were HADs, 25% of tumors were HCCs, and 41% were identified as CCs. In contrast, out of 185 tumor sections from the *Pten*^{LKO};*Tgfbr2*^{LKO} mice, a significantly different tumor profile as compared to the *Pten*^{LKO} mice was observed: 19% were HADs, 12% were HCCs, while 69% were CCs (P = 0.0019, 0.0027, 0.0001, respectively) (Table 2).

Presence of poorly differentiated liver tumors

Poorly differentiated tumors were noted in both genotypes, but were found to be more prevalent in the double knock-out mice. Specifically, 14 (N=14/185) were seen in the *Pten*^{LKO};*Tgfbr2*^{LKO} mice and 2 (N=2/157) were identified in the *Pten*^{LKO} mice (P = 0.0082, Fisher's exact test). These tumors were composed of poorly formed cords and trabeculae of anaplastic cells, with multifocal biliary ducts (Figure 3a and b). Additionally, these tumors lacked HepPar-1 staining of anaplastic tumor cells whereas, the biliary-like glands were positive for CK19 (Figure 3c and d). Interestingly, these tumors were diffusely positive for the stem cell marker c-Kit (CD117) (Figure 3e and f). It has been proposed that c-Kit positive hepatic progenitor cells have the potential to differentiate into hepatocytes and cholangiocytes and thus, the expression of c-Kit in these tumors suggests that the intermediate or poorly differentiated hepatic carcinomas arise from more primitive progenitor cells than do the cancers that are well differentiated HCCs and CC[37].

Loss of *Pten* and *Tgfbr2* result in alterations in various signaling pathways

Pten is a central negative regulator of the PI3K/AKT pathway. Thus, we assessed the activation status of this pathway in the tumors (T) and adjacent normal (N) liver tissue in the mice (Figure 4a). AKT phosphorylation was not detected in liver lysates from control or *Tgfbr2*^{LKO} mice. However, immunoblot analysis of liver tissue from both *Pten*^{LKO} and *Pten*^{LKO};*Tgfbf2*^{LKO} mice detected phosphorylated AKT on both Serine 473 and Threonine 308, indicating that AKT activation is independent of Tgfbr2 signaling, but increased in the face of Pten loss. We also assessed the phosphorylation status of the downstream kinase glycogen synthase kinase 3 beta (GSK-3β). GSK-3β is phosphorylated on Serine 9 in both the *Pten*^{LKO} and *Pten*^{LKO};*Tgfbf2*^{LKO} mice. For comparison, control and *Tgfbr2*^{LKO} mice

exhibited very low levels of GSK-3β phosphorylation. In many of the matched normal and tumor pairs, the phosphorylation of AKT (Ser 473) was modestly elevated in the tumor samples independent of the tumor type. We also assessed the activation status of the mTOR pathway (Figure 4b). Phosphorylation of mTOR at Serine 2448 was detected in all tissues, however slightly lower levels of phosphorylation were seen in the tumors of the double knock-out mice. Interestingly, phosphorylation of p70 S6 kinase at Serine 371 was observed in the liver tissue from the *Tgfbr2*^{LKO}, *Pten*^{LKO} and *Pten*^{LKO};*Tgfbf2*^{LKO} mice, indicating that both the TGF-β and PI3K/AKT/Pten pathways can affect the activation status of this pathway. Cyclin D1 has been found to be overexpressed in some human CCs[38]. Immunoblot analysis of tissues from our mouse models reveals that cyclin D1 is also upregulated in a subset of mouse liver tumors in the absence of Pten (Figure 4c). We also assessed SAPK/JNK pathway activation via c-Jun phosphorylation and found c-Jun phosphorylation on Serine 63 was increased in a subset of tumors from both *Pten*^{LKO} and *Pten*^{LKO};*Tgfbf2*^{LKO} mice (Supplementary Figure S2). MAPK pathway activation via Erk1/2 phosphorylation was also present in some tumors (Supplementary Figure S3).

Immunoblot analysis of phospho-Smad2 levels showed inter-tumor heterogeneity regardless of genotype. The presence of phospho-Smad2 in mice lacking *Tgfbr2* may be due to activin signaling (Supplementary Figure S4). We also assessed the localization of Smad4 in the liver tissue by IHC (Supplementary Figure S5). In normal hepatocytes, Smad4 staining is seen in the nucleus and cytoplasm. However, in HCCs from both genotypes the nuclear staining was decreased. Strong cytoplasmic staining was observed in the normal and tumor bile epithelium.

Alterations in the expression of hepatocyte and cholangiocyte specific genes

In light of the shift towards CCs in the *Pten*^{LKO};*Tgfbr2*^{LKO} mice, we sought to further characterize the gene expression profile of tumor and adjacent liver tissues isolated from mice of the various genotypes. We chose a set of hepatocyte, biliary, and stem cell markers. First, to verify our immunohistochemical results, we analyzed the expression of *CK19* (Figure 5a). As predicted, the CCs from the *Pten*^{LKO};*Tgfbr2*^{LKO} mice expressed significantly higher levels of *CK19* mRNA, compared to all the other tissues tested (P = 0.0385). Next, we analyzed the expression levels of alpha-fetoprotein (*Afp*) (Figure 5b). *Afp* is a gene that is frequently overexpressed in HCC (70%) and is a widely used clinical biomarker for HCC[39]. Consistent with the histological profiles, most *Pten*^{LKO} HCCs and HCCs with small adjacent CCs tumors expressed significantly higher levels of *Afp* compared to CCs and HCCs with adjacent CCs from *Pten*^{LKO};*Tgfbr2*^{LKO} mice (P = 0.0036). Next, we assessed the expression levels of cytokeratin 18 (*Krt18*), a gene known to be expressed in both hepatocytes and biliary epithelial cells (Figure 5c). We observed a significant increase in *Krt18* expression in the tumors of the *Pten*^{LKO} and *Pten*^{LKO};*Tgfbr2*^{LKO} mice, as compared to the control livers (P = 0.0003 and 0.0004, respectively). We also assessed the mRNA levels of the hepatocyte marker albumin (*Alb*) in normal and tumor liver tissues (Figure 5d). *Alb* levels were significantly lower in the tumor tissue from the *Pten*^{LKO} and *Pten*^{LKO};*Tgfbr2*^{LKO} mice compared to the normal control mice (P = 0.0040 and 0.0196, respectively), possibly the result of impaired liver function due to

steatosis. This observation has been described in human neoplastic liver tissue and has been associated with de-differentiated HCC and the loss of normal hepatocyte function[40].

Altered expression of stem cell markers in liver tissue from *Tgfbr2*^{LKO}, *Pten*^{LKO} and *Pten*^{LKO};*Tgfbr2*^{LKO} mice

Because the *Pten*^{LKO};*Tgfbr2*^{LKO} mice displayed a shift in liver tumor types, we assessed them for the expression of a subset of liver progenitor/stem cell markers (Figure 6). Scf and its receptor c-Kit play an important role in signal transduction in stem cells. In our mouse models, *c-Kit* expression was significantly higher in grossly and histologically normal liver tissue from *Tgfbr2*^{LKO} mice ($P = 0.0003$) compared to control mice (Figure 6a). This increase in *c-Kit* expression was also seen in the tumors from both the *Pten*^{LKO} and *Pten*^{LKO};*Tgfbr2*^{LKO} mice compared to controls ($P = 0.0019$ and <0.0001, respectively). Similarly, the expression of the stem cell marker *CD133* was also increased in the tissue from the *Tgfbr2*^{LKO} mice ($P = 0.0295$) compared to controls (Figure 6b). CD133 levels were further significantly increased in the tumors from the *Pten*^{LKO};*Tgfbr2*^{LKO} mice. Additionally, CD133 was also increased in normal tissue from the *Pten*^{LKO} and *Pten*^{LKO};*Tgfbr2*^{LKO} mice. This observation suggests that there is an expansion of a subset CD133+ liver cells in the *Tgfbr2*^{LKO}, *Pten*^{LKO}, and *Pten*^{LKO};*Tgfbr2*^{LKO} mice.

The expression levels of the ligand for c-Kit, *Scf*, were also measured in the liver tumors and adjacent normal tissue (Figure 6c). A significant increase in *Scf* levels was observed in the tumors from the *Pten*^{LKO} mice compared to adjacent normal tissue ($P = 0.0128$), however it was not significant when compared to the control or *Tgfbr2*^{LKO} mice ($P = 0.1020$ and 0.5809, respectively) or the normal tissue from the double mutants ($P = 0.4778$). In contrast, *Scf* levels were significantly increased in the tumors from the *Pten*^{LKO};*Tgfbr2*^{LKO} mice compared to its matched normal tissue ($P = 0.0056$), and normal tissue from the *Pten*^{LKO} ($P < 0.0001$), *Tgfbr2*^{LKO} ($P = 0.0003$) and control mice ($P = 0.0003$). The epithelial cell adhesion molecule EpCam is expressed in cholangiocytes of the adult liver and had also been detected in liver progenitor cells and cholangiocarcinomas[41]. There was a significant increase in *EpCam* expression in the *Pten*^{LKO};*Tgfbr2*^{LKO} tumors compared to adjacent normal tissue (Figure 6d, $P = 0.0068$). *EpCam* expression was also significantly increased in the normal tissue from the *Pten*^{LKO};*Tgfbr2*^{LKO} mice compared to the controls ($P < 0.0001$). Taken together, these data show an overall increase in stem cell markers in the double knock-out mice, but also highlight the importance of the loss of Tgfbr2 and Pten individually and their individual contributions to the overall phenotype.

Discussion

We have developed a mouse model for liver cancer that has allowed us to assess the *in vivo* functional interaction of *Pten* and *Tgfbr2* in the pathogenesis of this common form of cancer. We have found that liver specific deletion of *Pten* results in the formation of hepatic adenomas, hepatocellular carcinomas and cholangiocarcinomas in 67% of the mice by 12–14 months of age. Furthermore, inactivation of *Tgfbr2* in the setting of *Pten* loss increases the overall incidence of tumor formation in the mice to 86%, which suggests inactivation of TGF-β signaling cooperates with activated PI3K signaling to promote liver tumor formation.

We also observed that the loss of both *Pten* and *Tgfbr2* changed the distribution of the histologic tumor types induced by *Pten* inactivation alone. Specifically, there was a significant increase in the number of CCs that developed in the double KO livers as well as an overall increase in the expression of liver stem cell/progenitor markers including *c-Kit*, *CD133*, *Scf*, and *EpCam*.

The spectrum of tumors observed in the $Pten^{LKO}$;$Tgfbr2^{LKO}$ mice is similar to that reported for the $Pten^{LKO}$;$Smad4^{LKO}$ mice, in that they both developed a high number of CCs, which suggests that the TGF-β canonical SMAD pathway (as opposed to nonSmad TGF-β signaling pathways or activin or BMP mediated SMAD signaling) is the key pathway involved in the effects on CC formation[34]. However, in our model 56% of the $Pten^{LKO}$;$Tgfbr2^{LKO}$ mice developed both HAD/HCC and CCs within the same liver, whereas the $Pten^{LKO}$;$Smad4^{LKO}$ mice were reported to develop only CCs by 10 months[34]. Since Smad4 is shared between the TGF-β, BMP, activin, GDF, and Nodal signaling pathways, these results suggest the loss of Smad4 and deregulation of at least one of these other pathways results in a different phenotype than what we observed in our model in which only Tgfbr2 was inactivated. In our model BMP, activins, etc. are presumably still able to signal and could play a role in mediating cholangiocyte and hepatocyte specification.

Recently, intermediate liver carcinomas and hepatic stem cell malignancies have been reported[37]. These primary hepatic carcinomas share features between hepatocytes and cholangiocytes. Typically, these hybrid carcinomas often express hepatocytic markers such as HepPar-1, and cholangiocytic markers such as CK19. In our study, we found that the double knock-out mice developed more poorly differentiated tumors than the single $Pten^{LKO}$ mice and that these poorly differentiated tumors contained glandular structures that were positive for CK19, but also had anaplastic cells that were negative for both HepPar-1 and CK19. Interestingly, all of these cells were positive for c-Kit, suggesting that these tumors are derived from cells that have early stem-cell like features. Indeed, during liver regeneration, the expression of c-Kit is increased and thought to play a role in the activation of oval cells and hepatic stem cells[42,43]. These c-Kit positive hepatic progenitor cells have been proposed to have the ability to differentiate into both hepatocytes and cholangiocytes.

An interesting observation made in these studies is that although mice lacking functional Tgfbr2 do not develop liver tumors, they do exhibit changes in signaling pathways and gene expression. Specifically, mice lacking Tgfbr2 seem to have increased p70 S6 kinase phosphorylation. This increase may be due to loss of PP2A activation by TGF-β, and subsequent loss of PP2A inhibition of p70 S6 kinase phosphorylation, although this was not formally tested[44]. Deletion of Tgfbr2 also leads to the expression of a subset of progenitor/stem cell markers, namely *c-Kit* and *CD133*. Interestingly, a population of CD133+ tumor-initiating stem-like cells have been isolated from liver and found to be defective in TGF-β signaling[45].

In addition to providing insight into the signaling pathways that mediate the histologic types of cancers that form in the liver, the $Pten^{KO}$;$Tgfbr2^{KO}$ mouse also provides insight into the development of liver cancers that result from chronic inflammation in the liver. This is particularly relevant to human liver cancer that arises in the setting of steatohepatitis from

nonalcoholic fatty liver disease, which is dramatically increasing over the last two decades[46](Mittal and El-Serag 2013)[4646]. Previously published studies have demonstrated an association between chronic injury and expansion of the liver stem cell population as measured by hepatic progenitor markers such as c-Kit, CD133, EpCam, and others[16,19]. In our model, the loss of *Pten* and the resulting steatosis and accompanying reactive lipid products is believed to contribute to this chronic injury state and to the eventual development of HCC, CC, and poorly differentiated tumors. These studies have shown that loss of AKT2, in the setting of *Pten* deletion, inhibits the expansion and accumulation of these progenitor cells, providing evidence that the PI3K pathway is a regulator of liver stem cells. Interestingly, the number of liver tumors is decreased in the $Pten^{KO}$;$Akt2^{KO}$ mice but the tumor spectrum induced by Pten loss is not altered by the additional deletion of Akt2, which suggests that the PI3K pathway may regulate stem cell proliferation and not differentiation[19]. In contrast to the *Pten/Akt2* double knock-out mice, our $Pten^{LKO}$;$Tgfbr2^{LKO}$ mice display a significant change in the spectrum of tumors that develop when the TGF-β signaling pathway is disrupted in the setting of Pten loss. Specifically we see an increase in the number of CCs that develop, suggesting that TGF-β signaling inactivation in cooperation with PTEN/AKT signaling, induces cancer stem-like cells to differentiate towards a cholangiocyte fate. Furthermore, our results suggest that the biliary phenotype seen in the *Pten/Smad4* double knock-out mice is primarily due to the disruption of TGF-β signaling in the context of *Pten* loss. We also wish to note that there was substantial heterogeneity in the expression of the stem cell markers in the tumors in the $Pten^{LKO}$ and $Pten^{LKO}$;$Tgbr2^{LKO}$ mice which we believe reflects the effects of secondary somatic events in the tumors that differed between tumors. However, we cannot exclude the possibility that this may also reflect differences in the cell composition of the tumors (i.e. amount of tumor stroma vs. tumor epithelium).

It is clear that TGF-β signaling plays a complex role in liver development and tumor formation. Depending on the microenvironment and co-occurring mutations, TGF-β signaling has been shown to be both tumor suppressive and tumor promoting. In this study we provide evidence that TGF-β signaling is also important for tumor type specification. Specifically, inactivation of Tgfbr2 cooperates with loss of Pten to drive liver tumor formation primarily along the biliary lineage, resulting in the development of biliary hyperplasia and the eventual formation of CC. Understanding how various cytokines and growth factors affect the specification and differentiation of cancer stem cells will hopefully lead to more effective targeted therapies.

Methods

Mice

Alb-Cre transgenic mice (B6.Cg-Tg(Alb-cre)21Mgn) were crossed with $Pten^{flx/flx}$ mice (129S4-$Pten^{tm1Hwu}$/J2) and $Tgfbr2^{flx/flx}$ mice (B6.129S6-$Tgfbr2^{tm1Hlm}$) to generate the following: *Alb-Cre*;$Pten^{flx/flx}$;$Tgfbr2^{wt/wt}$ ($Pten^{LKO}$), *Alb-Cre*;$Pten^{wt/wt}$;$Tgfbr2^{flx/flx}$ ($Tgfbr2^{LKO}$), *Alb-Cre*;$Pten^{flx/flx}$;$Tgfbr2^{flx/flx}$ ($Pten^{LKO}$;$Tgfbr2^{LKO}$), and $Pten^{flx/flx}$;$Tgfbr2^{flx/flx}$ or $Pten^{flx/flx}$;$Tgfbr2^{wt/wt}$ (Control)[32,33,47,48]. Mice were from a mixed genetic background of C57BL6/129 and *Helicobacter* is known to be present in these colonies. Both male and

female mice were used. Genotypes were determined by PCR following published protocols[49]. Mice were maintained and cared for using protocols approved by the institutional IACUC. Mice that became moribund or reached approximately 14 months of age were sacrificed and necropsied.

Histology and immunohistochemical staining

Mouse liver tumors were noted grossly and specimens were fixed in 10% neutral buffered formalin (Fisher Scientific, Pittsburgh, PA, USA), embedded in paraffin, and cut into 4 um sections for H&E and immunostaining. Liver tumors were classified based on published descriptions[50,51].

For immunohistochemistry, tissue sections were stained with antibodies against HepPar-1 (1:75, Clone OCH1E5, Dako, Glostrup, Denmark), c-Kit (1:100, sc-168, Santa Cruz Biotechnology, Inc., Dallas, TX, USA), CK19 (1:50, TROMA-III-c, University of Iowa, Iowa City, IA, USA), and Smad4 (1:50, 1676-1, Epitomics, Burlingame, CA, USA). Tissue staining was developed with DAB and counterstained with hematoxylin. Images were captured from whole-slide images acquired with the Aperio ScanScope AT (Aperio, Carlsbad, CA, USA) using the 20X objective. Examination of H&E stained sections was performed by pathologists blinded to genotype. Assays were performed in the Experimental Histopathology Core at the Fred Hutchinson Cancer Research Center following routine laboratory protocols. Specific protocols are available upon request.

Immunoblot analyses

The tumor samples were grossly dissected and were randomly selected from multiple mice within the indicated genotype. Total protein lysates were prepared from frozen tumor and non-tumor liver tissue as previously described[52]. Lysates (30 ug per lane) were resolved by 10% SDS-PAGE and transferred to PVDF membranes (Thermo Scientific, Rockford, IL, USA). The following antibodies were used: Rabbit anti-GAPDH conjugated to horseradish peroxidase (HRP) (1:10,000, #3683 Cell Signaling, Danvers, MA, USA), Rabbit anti-Akt (1:1000, #9272, Cell Signaling), Rabbit anti-Phospho-Akt, Ser473 (1:1000, #9271, Cell Signaling), Rabbit anti-Phospho-Akt, Thr308 (1:1000, #9275, Cell Signaling), Rabbit anti-GSK-3β (1:1000, #9315, Cell Signaling), Rabbit anti-GSK-3β, Ser9 (1:1000, #9323, Cell Signaling), Rabbit anti-Phospho-mTOR Ser2448 (1:1000, #2971, Cell Signaling), Rabbit anti-Phospho-p70 S6 Kinase Ser371 (1:1000, #9208, Cell Signaling), Mouse anti-Cyclin D1 (1:2000, #2926, Cell Signaling), Rabbit anti-Phospho-Smad2 (1:1000, #3101, Cell Signaling), Rabbit anti-Smad2/3 (#3102, 1:1000, Cell Signaling), Rabbit anti-Beta-Actin (1:2000, #4970, Cell Signaling), Goat anti-Rabbit IgG-HRP (1:5,000, #SC-2004, Santa Cruz Biotechnology, Inc.) and Goat anti-Mouse IgG-HRP (1:5,000, #SC-2005, Santa Cruz). Densitometric quantification of immunoblots was performed using the ImageJ 1.45 software.

Real-time quantitative reverse transcription polymerase chain reaction (qRT-PCR)

Taqman gene expression assays (Life Technologies, Grand Island, NY, USA) for keratin 19 (CK19, Krt19: Mm00492980_m1), alpha-fetoprotein (AFP: Mm00431715_m1), keratin 18 (Krt18:Mm01601704_g1), albumin (Alb: Mm00802090_m1), epithelial cell adhesion

molecule (EpCAM: Mm00493214_m1), stem cell factor receptor (c-Kit: Mm00445212_m1), stem cell factor (Scf, Kitl: Mm00442972_m1), and CD133 (Prom1: Mm00477115_m1) were used for qRT-PCR. Beta 2 Microglobulin (B2M: Mm00437762_m1) was used as a control. mRNA was extracted from snap-frozen tissues using TRIzol (Life Technologies, Carlsbad, CA, USA) following the manufacturer's instructions. cDNA was generated using standard procedures using oligodT primers (Life Technologies). Real-time assays were performed using the SsoFast Probes Supermix (Bio-Rad, Hercules, CA, USA) and run on a Bio-Rad CFX96 real-time PCR system. Statistical analysis was performed using GraphPad Prism version 6.02. The Mann-Whitney test was used for comparison of quantitative results from the qRT-PCR assays. A P value of <0.05 was regarded as significant.

Supplementary Material

Refer to Web version on PubMed Central for supplementary material.

Acknowledgements

This work supported in part by funding from Burroughs Wellcome Fund, the National Institutes of Health (RO1 DK60669-01 and P30 CA015704, WMG) and by the National Institutes of Health Interdisciplinary Training Grant (T32 CA080416, SMM). The authors thank Jean Campbell and members of the Grady laboratory for helpful suggestions. We also wish to acknowledge support from the Experimental Histopathology, Scientific Imaging, and Comparative Medicine Cores at the Fred Hutchinson Cancer Research Center.

References

1. Jemal A, Bray F, Center MM, Ferlay J, Ward E, Forman D. Global cancer statistics. CA Cancer J Clin. 2011; 61:69–90. [PubMed: 21296855]
2. Singal AK, Vauthey JN, Grady JJ, Stroehlein JR. Intra-hepatic cholangiocarcinoma--frequency and demographic patterns: thirty-year data from the M.D. Anderson Cancer Center. J Cancer Res Clin Oncol. 2011; 137:1071–1078. [PubMed: 21207060]
3. Yeh MM. Pathology of combined hepatocellular-cholangiocarcinoma. J Gastroenterol Hepatol. 2010; 25:1485–1492. [PubMed: 20796144]
4. Wu, X.; Li, Y. Julianov, A., editor. Signaling Pathways in Liver Cancer; Liver Tumors. 2012. p. 37-58.www.intechopen.com: InTech
5. Majumdar A, Curley SA, Wu X, Brown P, Hwang JP, Shetty K, et al. Hepatic stem cells and transforming growth factor beta in hepatocellular carcinoma. Nat Rev Gastroenterol Hepatol. 2012; 9:530–538. [PubMed: 22710573]
6. Fabregat I. Dysregulation of apoptosis in hepatocellular carcinoma cells. World J Gastroenterol. 2009; 15:513–520. [PubMed: 19195051]
7. Breuhahn K, Longerich T, Schirmacher P. Dysregulation of growth factor signaling in human hepatocellular carcinoma. Oncogene. 2006; 25:3787–3800. [PubMed: 16799620]
8. Whittaker S, Marais R, Zhu AX. The role of signaling pathways in the development and treatment of hepatocellular carcinoma. Oncogene. 2010; 29:4989–5005. [PubMed: 20639898]
9. Chalhoub N, Baker SJ. PTEN and the PI3-kinase pathway in cancer. Annu Rev Pathol. 2009; 4:127–150. [PubMed: 18767981]
10. Carracedo A, Pandolfi PP. The PTEN-PI3K pathway: of feedbacks and cross-talks. Oncogene. 2008; 27:5527–5541. [PubMed: 18794886]
11. Shi Y, Paluch BE, Wang X, Jiang X. PTEN at a glance. J Cell Sci. 2012; 125:4687–4692. [PubMed: 23223894]
12. Yao YJ, Ping XL, Zhang H, Chen FF, Lee PK, Ahsan H, et al. PTEN/MMAC1 mutations in hepatocellular carcinomas. Oncogene. 1999; 18:3181–3185. [PubMed: 10340391]

13. Hu TH, Huang CC, Lin PR, Chang HW, Ger LP, Lin YW, et al. Expression and prognostic role of tumor suppressor gene PTEN/MMAC1/TEP1 in hepatocellular carcinoma. Cancer. 2003; 97:1929–1940. [PubMed: 12673720]
14. Forbes SA, Bhamra G, Bamford S, Dawson E, Kok C, Clements J, et al. The Catalogue of Somatic Mutations in Cancer (COSMIC). Curr Protoc Hum Genet. 2008; Chapter 10(Unit 10):11. [PubMed: 18428421]
15. Knobbe CB, Lapin V, Suzuki A, Mak TW. The roles of PTEN in development, physiology and tumorigenesis in mouse models: a tissue-by-tissue survey. Oncogene. 2008; 27:5398–5415. [PubMed: 18794876]
16. Rountree CB, Ding W, He L, Stiles B. Expansion of CD133-expressing liver cancer stem cells in liver-specific phosphatase and tensin homolog deleted on chromosome 10-deleted mice. Stem Cells. 2009; 27:290–299. [PubMed: 19008348]
17. Stiles B, Wang Y, Stahl A, Bassilian S, Lee WP, Kim YJ, et al. Liver-specific deletion of negative regulator Pten results in fatty liver and insulin hypersensitivity [corrected]. Proc Natl Acad Sci USA. 2004; 101:2082–2087. [PubMed: 14769918]
18. Horie Y, Suzuki A, Kataoka E, Sasaki T, Hamada K, Sasaki J, et al. Hepatocyte-specific Pten deficiency results in steatohepatitis and hepatocellular carcinomas. J Clin Invest. 2004; 113:1774–1783. [PubMed: 15199412]
19. Galicia VA, He L, Dang H, Kanel G, Vendryes C, French BA, et al. Expansion of hepatic tumor progenitor cells in Pten-null mice requires liver injury and is reversed by loss of AKT2. Gastroenterology. 2010; 139:2170–2182. [PubMed: 20837017]
20. Amin R, Mishra L. Liver stem cells and tgf-Beta in hepatic carcinogenesis. Gastrointest Cancer Res. 2008; 2:S27–30. [PubMed: 19343145]
21. Herrera B, Sanchez A, Fabregat I. BMPS and liver: more questions than answers. Curr Pharm Des. 2012; 18:4114–4125. [PubMed: 22630083]
22. Zaret KS. Hepatocyte differentiation: from the endoderm and beyond. Curr Opin Genet Dev. 2001; 11:568–574. [PubMed: 11532400]
23. Clotman F, Jacquemin P, Plumb-Rudewiez N, Pierreux CE, Van der Smissen P, Dietz HC, et al. Control of liver cell fate decision by a gradient of TGF beta signaling modulated by Onecut transcription factors. Genes Dev. 2005; 19:1849–1854. [PubMed: 16103213]
24. Wu K, Ding J, Chen C, Sun W, Ning BF, Wen W, et al. Hepatic transforming growth factor beta gives rise to tumor-initiating cells and promotes liver cancer development. Hepatology. 2012; 56:2255–2267. [PubMed: 22898879]
25. Shiraki N, Umeda K, Sakashita N, Takeya M, Kume K, Kume S. Differentiation of mouse and human embryonic stem cells into hepatic lineages. Genes Cells. 2008; 13:731–746. [PubMed: 18513331]
26. Cai J, Zhao Y, Liu Y, Ye F, Song Z, Qin H, et al. Directed differentiation of human embryonic stem cells into functional hepatic cells. Hepatology. 2007; 45:1229–1239. [PubMed: 17464996]
27. Kitisin K, Ganesan N, Tang Y, Jogunoori W, Volpe EA, Kim SS, et al. Disruption of transforming growth factor-beta signaling through beta-spectrin ELF leads to hepatocellular cancer through cyclin D1 activation. Oncogene. 2007; 26:7103–7110. [PubMed: 17546056]
28. Bierie B, Moses HL. TGF-beta and cancer. Cytokine Growth Factor Rev. 2006; 17:29–40. [PubMed: 16289860]
29. Attisano L, Wrana JL. Signal integration in TGF-beta, WNT, and Hippo pathways. F1000Prime Rep. 2013; 5:17. [PubMed: 23755364]
30. Peyrou M, Bourgoin L, Foti M. PTEN in liver diseases and cancer. World J Gastroenterol. 2010; 16:4627–4633. [PubMed: 20872961]
31. Hollander MC, Blumenthal GM, Dennis PA. PTEN loss in the continuum of common cancers, rare syndromes and mouse models. Nat Rev Cancer. 2011; 11:289–301. [PubMed: 21430697]
32. Postic C, Magnuson MA. DNA excision in liver by an albumin-Cre transgene occurs progressively with age. Genesis. 2000; 26:149–150. [PubMed: 10686614]
33. Lesche R, Groszer M, Gao J, Wang Y, Messing A, Sun H, et al. Cre/loxP-mediated inactivation of the murine Pten tumor suppressor gene. Genesis. 2002; 32:148–149. [PubMed: 11857804]

34. Xu X, Kobayashi S, Qiao W, Li C, Xiao C, Radaeva S, et al. Induction of intrahepatic cholangiocellular carcinoma by liver-specific disruption of Smad4 and Pten in mice. J Clin Invest. 2006; 116:1843–1852. [PubMed: 16767220]
35. Wakefield LM, Hill CS. Beyond TGFbeta: roles of other TGFbeta superfamily members in cancer. Nat Rev Cancer. 2013; 13:328–341. [PubMed: 23612460]
36. Wennerberg AE, Nalesnik MA, Coleman WB. Hepatocyte paraffin 1: a monoclonal antibody that reacts with hepatocytes and can be used for differential diagnosis of hepatic tumors. Am J Pathol. 1993; 143:1050–1054. [PubMed: 7692729]
37. Kim H, Park C, Han KH, Choi J, Kim YB, Kim JK, et al. Primary liver carcinoma of intermediate (hepatocyte-cholangiocyte) phenotype. J Hepatol. 2004; 40:298–304. [PubMed: 14739102]
38. Sugimachi K, Aishima S, Taguchi K, Tanaka S, Shimada M, Kajiyama K, et al. The role of overexpression and gene amplification of cyclin D1 in intrahepatic cholangiocarcinoma. J Hepatol. 2001; 35:74–79. [PubMed: 11495045]
39. Zhou L, Liu J, Luo F. Serum tumor markers for detection of hepatocellular carcinoma. World J Gastroenterol. 2006; 12:1175–1181. [PubMed: 16534867]
40. Luo SM, Tan WM, Deng WX, Zhuang SM, Luo JW. Expression of albumin, IGF-1, IGFBP-3 in tumor tissues and adjacent non-tumor tissues of hepatocellular carcinoma patients with cirrhosis. World J Gastroenterol. 2005; 11:4272–4276. [PubMed: 16015705]
41. Yamashita T, Wang XW. Cancer stem cells in the development of liver cancer. J Clin Invest. 2013; 123:1911–1918. [PubMed: 23635789]
42. Mansuroglu T, Baumhoer D, Dudas J, Haller F, Cameron S, Lorf T, et al. Expression of stem cell factor receptor c-kit in human nontumoral and tumoral hepatic cells. Eur J Gastroenterol Hepatol. 2009; 21:1206–1211. [PubMed: 19491699]
43. Mansuroglu T, Ramadori P, Dudas J, Malik I, Hammerich K, Fuzesi L, et al. Expression of stem cell factor and its receptor c-Kit during the development of intrahepatic cholangiocarcinoma. Lab Invest. 2009; 89:562–574. [PubMed: 19255573]
44. Petritsch C, Beug H, Balmain A, Oft M. TGF-beta inhibits p70 S6 kinase via protein phosphatase 2A to induce G(1) arrest. Genes Dev. 2000; 14:3093–3101. [PubMed: 11124802]
45. Chen CL, Tsukamoto H, Liu JC, Kashiwabara C, Feldman D, Sher L, et al. Reciprocal regulation by TLR4 and TGF-beta in tumor-initiating stem-like cells. J Clin Invest. 2013; 123:2832–2849. [PubMed: 23921128]
46. Mittal S, El-Serag HB. Epidemiology of hepatocellular carcinoma: consider the population. J Clin Gastroenterol. 2013; 47(Suppl):S2–6. [PubMed: 23632345]
47. Postic C, Shiota M, Niswender KD, Jetton TL, Chen Y, Moates JM, et al. Dual roles for glucokinase in glucose homeostasis as determined by liver and pancreatic beta cell-specific gene knock-outs using Cre recombinase. J Biol Chem. 1999; 274:305–315. [PubMed: 9867845]
48. Chytil A, Magnuson MA, Wright CV, Moses HL. Conditional inactivation of the TGF-beta type II receptor using Cre:Lox. Genesis. 2002; 32:73–75. [PubMed: 11857781]
49. Romero-Gallo J, Sozmen EG, Chytil A, Russell WE, Whitehead R, Parks WT, et al. Inactivation of TGF-beta signaling in hepatocytes results in an increased proliferative response after partial hepatectomy. Oncogene. 2005; 24:3028–3041. [PubMed: 15735717]
50. Thoolen B, Maronpot RR, Harada T, Nyska A, Rousseaux C, Nolte T, et al. Proliferative and nonproliferative lesions of the rat and mouse hepatobiliary system. Toxicol Pathol. 2010; 38:5S–81S. [PubMed: 21191096]
51. Deschl, U.; Cattley, R.; Harada, T.; Kuttler, K.; Hailey, J.; Hartig, F.; Leblanc, B.; Marsman, D.; Shirai, T. Liver, gallbladder and exocrine pancreas. In: Mohr, U., editor. International classification of rodent tumors: The mouse. Springer Verlag; Heidelberg, Germany: 2001. p. 59-86.
52. Morris SM, Baek JY, Koszarek A, Kanngurn S, Knoblaugh SE, Grady WM. Transforming growth factor-beta signaling promotes hepatocarcinogenesis induced by p53 loss. Hepatology. 2012; 55:121–131. [PubMed: 21898503]

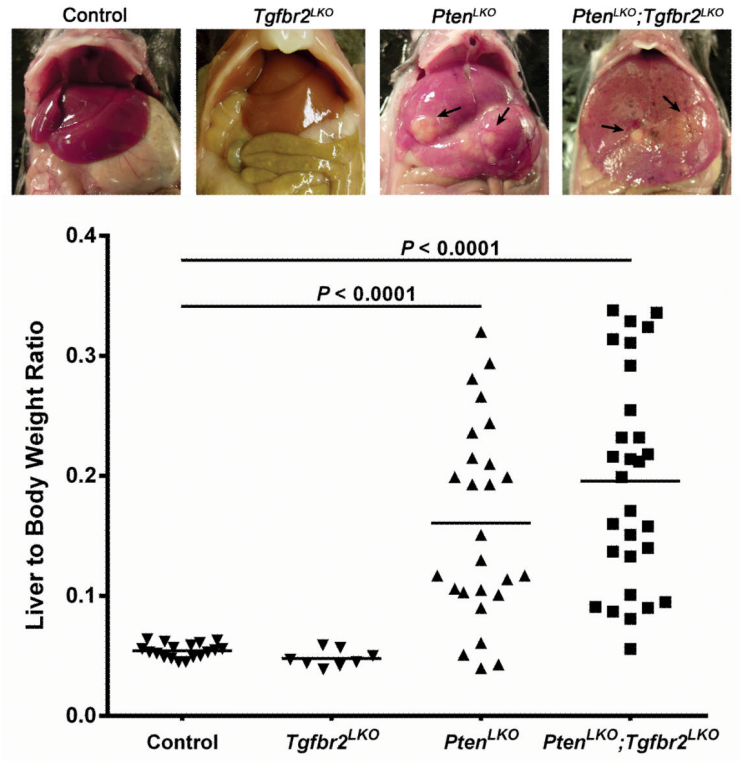

Figure 1.

Liver to body weight ratios. Upper panels show representative images of livers from the various genotypes at approximately 1 year of age. Arrows indicate grossly visible tumors in the *Pten*^{LKO} and *Pten*^{LKO};*Tgfbr2*^{LKO} mice. Both the *Pten*^{LKO} and the *Pten*^{LKO};*Tgfbr2*^{LKO} mice displayed a significant increase in liver to body weight ratios as compared to *Tgfbr2*^{LKO} and control mice ($P < 0.0001$). However, there was no significant difference between the liver to body weight ratios of the *Pten*^{LKO} and the *Pten*^{LKO};*Tgfbr2*^{LKO} mice ($P = 0.1618$).

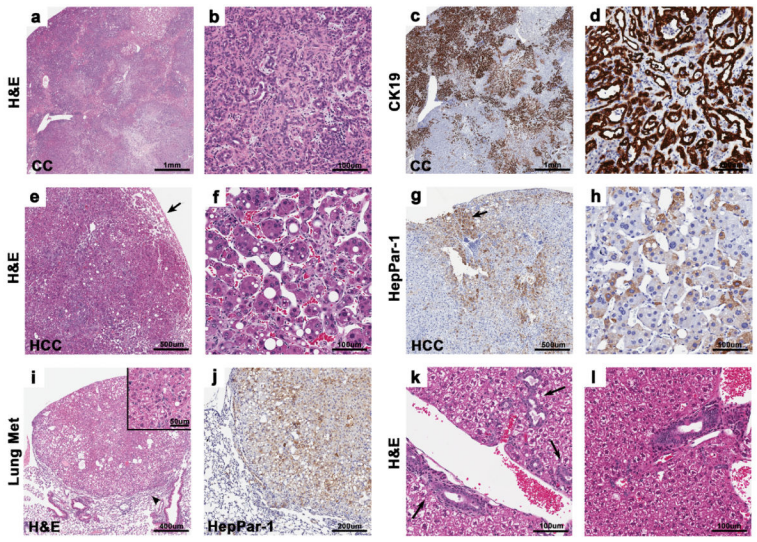

Figure 2.

Histology of representative liver tumors and lung metastasis. (**a**) Coalescing CCs and areas of biliary hyperplasia occupy the entire liver lobe of a $Pten^{LKO};Tgfbr2^{LKO}$ mouse, 2X. (**b**) Higher magnification of a CC in "a" consisting of irregular tubules and glands, 20X. (**c**) Positive CK19 staining of coalescing biliary lesions in "a", 2X. (**d**) Higher magnification of CC positively stained with CK19, 20X. (**e**) Large HCC from a $Pten^{LKO}$ mouse with invasion into adjacent parenchyma (arrow), 4X. (**f**) Higher magnification of HCC in "e" with prominent trabecular formation, 20X. (**g**) Heterogeneous HepPar-1 staining of an HCC from a $Pten^{LKO}$ mouse. There is multifocal positive staining of HCC neoplastic cells and positive staining of the normal hepatocytes at the periphery (arrow), 4X. (**h**) HepPar-1 immunostaining of HCC showing cytoplasmic positivity in many tumor cells, 20X. (**i**) HCC metastasis to the lung from a $Pten^{LKO};Tgfbr2^{LKO}$ mouse, 5X. Note the compression of the adjacent pulmonary parenchyma (arrowhead). Inset, higher magnification of lung tumor, 20X. (**j**) Lung section with hepatocyte specific marker, HepPar-1, positive metastasis 10X. (**k**) Multifocal biliary hyperplasia and biliary epithelial hypertrophy in 18 week old $Pten^{LKO};Tgfbr2^{LKO}$ mice. Note the increase in bile ducts (arrows), 20X. (**l**) Mild biliary hyperplasia and diffuse biliary epithelial hypertrophy in young *Pten* null liver, 20X.

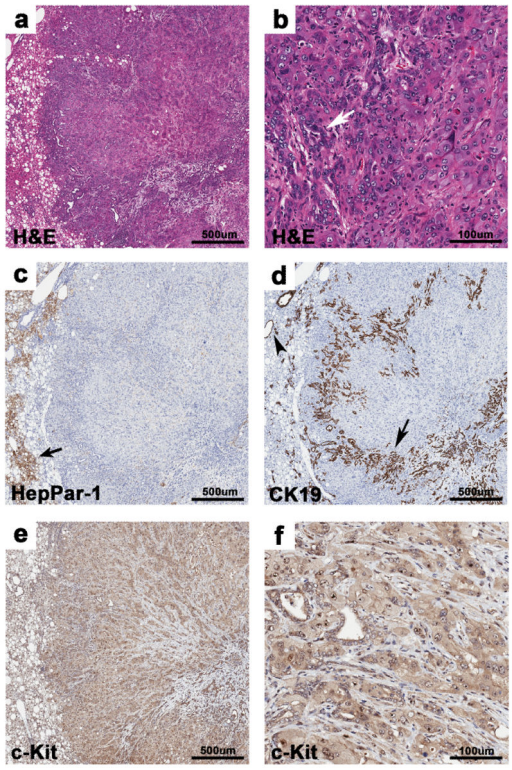

Figure 3.

Poorly differentiated liver tumors. (**a**) Poorly differentiated liver tumor from a $Pten^{LKO};Tgfbr2^{LKO}$ mouse composed of poorly formed cords and trabeculae, with multifocal irregular glands, 4X. (**b**) Higher magnification of “a”. Poorly formed cords and trabeculae of anaplastic cells with multifocal, irregular glands (white arrow), 20X. (**c**) Absence of HepPar-1 staining in the tumor is shown. Note the adjacent positive staining in normal hepatocytes, arrow, 4X. (**d**) Normal bile ducts in adjacent parenchyma (arrowhead) and glandular structures within the tumor (arrow) stain positive for the cholangiocyte marker CK19, 4X. (**e**) Within the poorly differentiated carcinoma, anaplastic cells and glands are positive for c-Kit, 4X. (**f**) Higher magnification of “e” showing c-Kit staining, 20X.

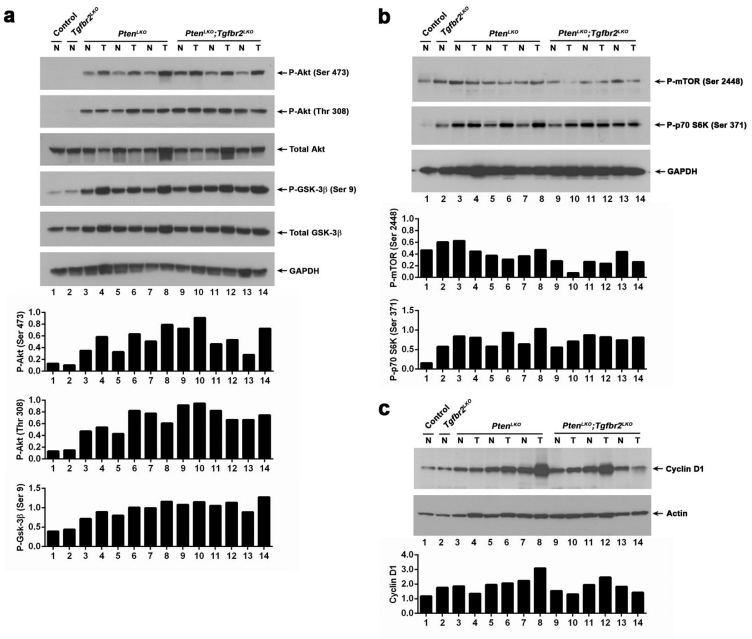

Figure 4.

Signaling pathway alterations. (**a**) Upper panels, analysis of Akt phosphorylation by immunoblot demonstrates an increase in phospho-Akt (P-Akt) at both serine 473 and threonine 308 in normal (N) and tumor (T) liver tissues from *Pten*^{LKO} (P^{LKO}) and *Pten*^{LKO};*Tgfbr2*^{LKO} (T;P^{LKO}) mice, but not in tissues from control or *Tgfbr2*^{LKO} (T^{LKO}) mice. Similarly, an increase in the phosphorylation of GSK-3β at serine 9 was also observed in the *Pten*^{LKO} and *Pten*^{LKO};*Tgfbr2*^{LKO} liver tissues. GAPDH was used as a loading control. Lower panels, quantitation of phosphorylation as determined by densitometry; phospho-AKT normalized to total AKT, and then GAPDH; phospho-GSK-3β normalized to total GSK-3β, and then GAPDH. (**b**) Upper panels, analysis of mTOR and p70 S6 kinase phosphorylation in normal and tumor tissue. GAPDH was used as a loading control. Lower panels, quantitation of phosphorylation as determined by densitometry; phospho-mTOR or phospho-p70 S6 kinase and then GAPDH. (**c**) Upper panels, analysis of cyclin D1 protein expression in normal and tumor liver tissue. Actin was used as a loading control. Lower panel, quantitation of cyclin D1 levels normalized to actin.

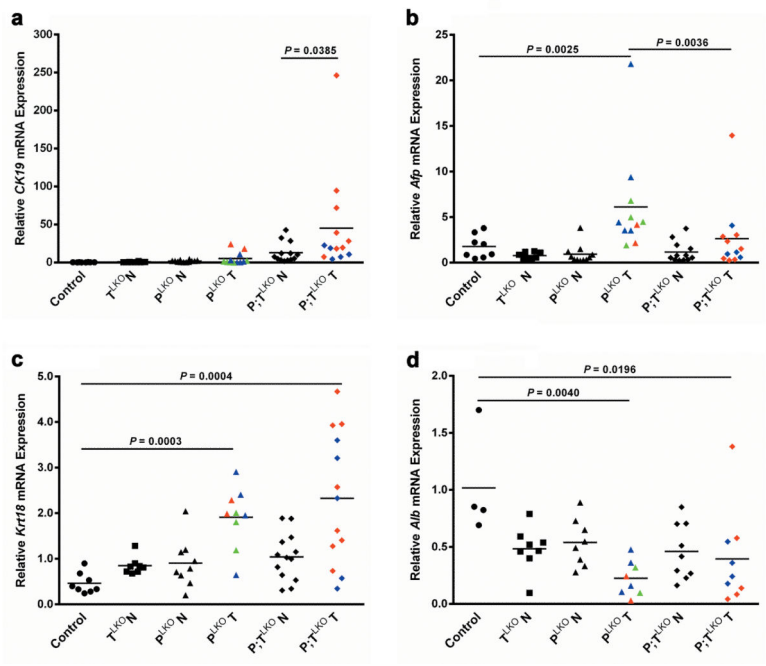

Figure 5.

Expression of HCC and CC related genes in *Tgfbr2*^{LKO} (*T*^{LKO}), *Pten*^{LKO} (*P*^{LKO}) and *Pten*^{LKO};*Tgfbr2*^{LKO} (*P;T*^{LKO}) mice. (**a**) qRT-PCR analysis reveals that *CK19* mRNA levels are increased in the tumor tissue (T) from the *P;T*^{LKO} vs. the adjacent normal tissue (N) (*P* = 0.0385). (**b**) *Afp* mRNA levels are increased in the tumors from the *P*^{LKO} mice compared to the tumors from the *P;T*^{LKO} mice (*P* = 0.0036) and control mice (*P* = 0.0025). (**c**) *Krt18* mRNA levels are increased in liver tumors from both the *P*^{LKO} and *P;T*^{LKO} mice compared control livers (*P* = 0.0003 and 0.0004, respectively). (**d**) *Alb* mRNA expression is decreased significantly in the tumor tissue from both the *P*^{LKO} and *P;T*^{LKO} mice compared to the normal control livers (*P* = 0.0040 and 0.0196, respectively). Color code of tumor histology: Red = CC, Green = HCC, Blue = Tumors with both HCC/CC components.

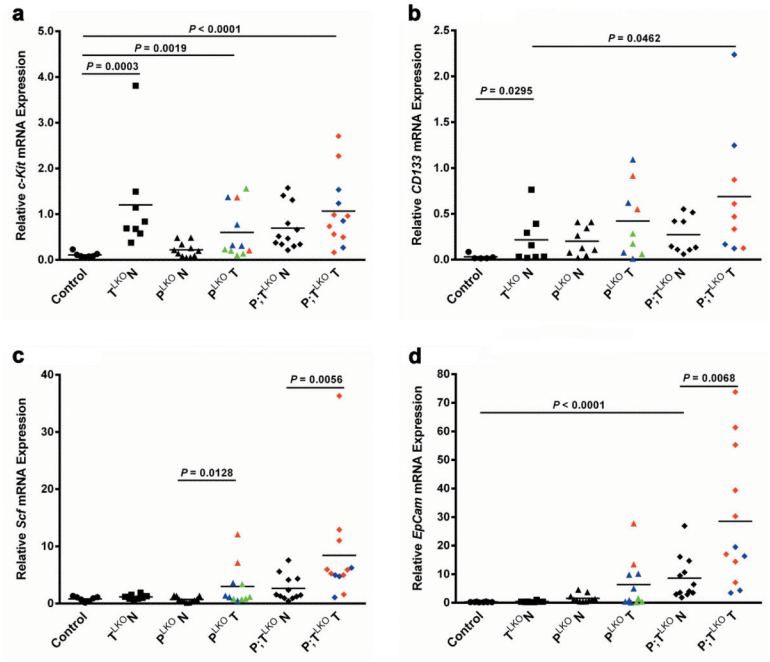

Figure 6.

Expression of liver progenitor/stem cell markers. (**a**) qRT-PCR analysis reveals that *c-Kit* mRNA levels are increased in the normal tissue (N) from the T^{LKO} vs. control livers (P = 0.0003). Additionally, *c-Kit* levels in the tumor tissue (T) from both the P^{LKO} and $P;T^{LKO}$ mice are significantly higher than control livers (P = 0.0019 and < 0.0001, respectively). (**b**) *CD133* mRNA expression is increased in the tissue from the T^{LKO} vs. normal control livers (P = 0.0295). The level of CD133 expression is further increased in the tumors from the $P;T^{LKO}$ mice (P = 0.0462). (**c**) *Scf* mRNA levels are increased in the tumors from the P^{LKO} mice compared to normal adjacent tissue from P^{LKO} mice (P = 0.0128). *Scf* is also increase in the tumor tissue from the $P;T^{LKO}$ mice compared to normal adjacent tissue (P = 0.0056). (**d**) *EpCam* mRNA levels in the tumors from the $P;T^{LKO}$ mice are higher than the adjacent normal tissue (P = 0.0068). Color code of tumor histology: Red = CC, Green = HCC, Blue = Tumors with both HCC/CC components.

Table 1

Tumor Incidence in Mice

Summary of Mice Used				Tumor Types in Mice with Hepatic Tumors			
Genotype	**# of Mice**	**Avg. Age (wks)**	**# of Mice w/ Hepatic Tumors**	**HAD/HCC**	**cc**	**HAD/HCC & CC**	**Lung Mets**
Control (No *Alb-Cre*)	19 (9M/10F)	58.9	0	0	0	0	0
Tgfbr2^{LKO}	8 (4M/4F)	66.5	0	0	0	0	0
Pten^{LKO}	30 (15M/15F)	54.9	20 (67%)	3 (15%)	2[1] (10%)	15 (75%)	0
Pten^{LKO};*Tgfbr2*^{LKO}	29 (9M/20F)	59.4	25 (86%)	0	11[1] (44%)	14 (56%)	1

[1] $P = 0.0197$, *Pten*^{LKO} (2/20) vs. *Pten*^{LKO};*Tgfbr2*^{LKO} (11/25), Fisher's exact test, two-tailedHAD= hepatic adenoma; HCC=hepatocellular carcinoma, CC=cholangiocarcinoma, M=male, F=female

Table 2

Summary of Individual Tumors by Histology

Genotype	# of Tumors Scored	HAD	HCC	CC
Pten^{LKO}	157	53[1] (34%)	39[2] (25%)	65[3] (41%)
Pten^{LKO};*Tgfbr2*^{LKO}	185	35[1] (19%)	22[2] (12%)	128[3] (69%)

[1] $P = 0.0019$, *Pten*^{LKO}(53/157) vs. *Pten*^{LKO};*Tgfbr2*^{LKO} (35/185), Fisher's exact test, two-tailed

[2] $P = 0.0027$, *Pten*^{LKO}(39/157) vs. *Pten*^{LKO};*Tgfbr2*^{LKO} (22/185), Fisher's exact test, two-tailed

[3] $P < 0.0001$, *Pten*^{LKO}(65/157) vs. *Pten*^{LKO};*Tgfbr2*^{LKO} (128/185), Fisher's exact test, two-tailed